PROCEEDINGS OF SCIENCE

Recent results from BESIII

Shuangshi FANG[*†]
Institute of High Energy Physics, CAS, Beijing, 100049, China
E-mail: fangss@ihep.ac.cn

Based on the samples of 106 million ψ' events, 225 million J/ψ events and 2.9 fb^{-1} of $\psi(3773)$ collected at the BESIII detector, the recent results on charmonium decays, light hadron spectroscopy and charm decays are presented.

The 7th International Workshop on Chiral Dynamics,
August 6 -10, 2012
Jefferson Lab, Newport News, Virginia, USA

[*]Speaker.
[†]On behalf of the BESIII Collaboration

PoS(CD12)005

1. Introduction

To meet the challenge of precision measurements of $\tau-$charm physics, a major upgrade on the Beijing Electron-Positron Collider (BEPC) and the Beijing Spectrometer (BES) has been completed in 2008 (called BEPCII and BESIII afterwards). The BEPCII is a double ring e^+e^- collider. The design peak luminosity is 10^{33} cm$^{-2}s^{-1}$ at 3.773 GeV, which is 100 times better than its predecessor. In this talk the recent results on charmonium decays, light hadron spectroscopy and charm decays are presented with the samples of 106 million ψ' events, 225 million J/ψ events and 2.9 fb^{-1} of $\psi(3770)$ collected at the BESIII detector.

2. Measurement of the η_c properties [1]

In this analysis, the mass and width of η_c are measured via ψ' radiative decays, where η_c are reconstructed from six decay modes: $K^0_SK\pi$, $K^+K^-\pi^0$, $\pi^+\pi^-\eta$, $K^0_SK3\pi$, $K^+K^-\pi^+\pi^-\pi^0$ and $3(\pi^+\pi^-)$. For the first time, the interference between the η_c and the non-resonant amplitudes around the η_c mass is considered, which has a significant impact on the η_c mass and width. A simultaneous fit is performed on the η_c mass spectra shown in Fig. 1, where the interference between η_c and non-resonance decays is considered and the quantum number of the non-η_c components are assumed to be 0^{-+}. Assuming an universal relative phase between the two amplitudes, we obtain η_c mass and width, $M = 2984.2 \pm 0.6 \pm 0.6$ MeV/c^2 and $\Gamma = 32.0 \pm 1.2 \pm 1.0$ MeV/c^2, respectively, which are so far the most precise single measurement of the mass and width of η_c.

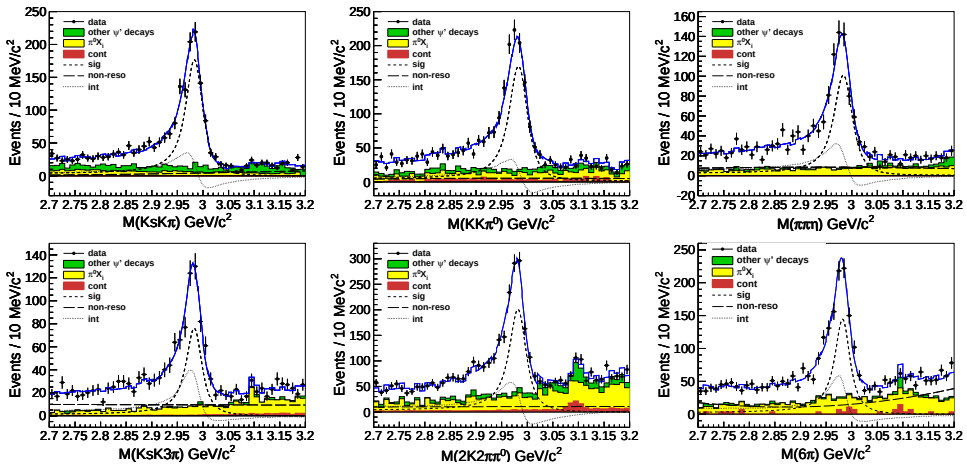

Figure 1: The mass spectra for different decay modes, where the line is the result of the simultaneous fit.

3. Observation of h_c [2]

We present measurements of the charmonium state $h_c(^1P_1)$ made with 106 million ψ'. Clear h_c signals are observed for $\psi' \to \pi^0 h_c$ with and without the subsequent radiative decay $h_c \to \gamma\eta_c$, which are shown in Fig. 2(a) and Fig. 2(b), respectively. First measurements of the absolute branching ratios $\mathscr{B}(\psi' \to \pi^0 h_c) = (8.4 \pm 1.3 \pm 1.0) \times 10^{-4}$ and $\mathscr{B}(h_c \to \gamma\eta_c) = (54.3 \pm 6.7 \pm 5.2)\%$ are

presented. A statistics-limited determination of the previously unmeasured h_c width leads to an upper limit $\Gamma(h_c) < 1.44$ MeV (90% confidence). Measurements of $M(h_c) = 3525.40 \pm 0.13 \pm 0.18$ MeV/c^2 and $\mathscr{B}(\psi' \to \pi^0 h_c) \times \mathscr{B}(h_c \to \gamma\eta_c) = (4.58 \pm 0.40 \pm 0.50) \times 10^{-4}$ are consistent with previous results.

We also performed a study of the 16 specific decay processes of η_c in the decay chain of $\psi' \to \pi^0 h_c$, $h_c \to \gamma\eta_c$. A simultaneous fit to the 16 π^0 recoil-mass spectra yields $M(h_c) = 3525.31 \pm 0.11 \pm 0.15\text{MeV}/c^2$ and $\Gamma(h_c) = 0.70 \pm 0.28 \pm 0.25\text{MeV}/c^2$. These preliminary results are consistent with the above BESIII measurements.

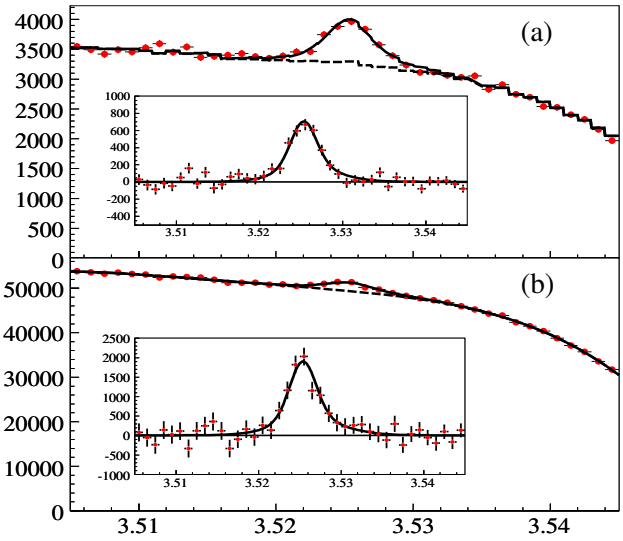

Figure 2: (a) The π^0 recoil mass spectrum and fit for the $E1$-tagged analysis of $\psi' \to \pi^0 h_c, h_c \to \gamma\eta_c$; (b) the π^0 recoil mass spectrum and fit for the inclusive analysis of $\psi' \to \pi^0 h_c$. Fits are shown as solid lines, background as dashed lines. The insets show the background-subtracted spectra.

4. First observation of the M1 transition $\psi' \to \gamma\eta_c(2S)$ [3]

The first measurement of the M1 transition process $\psi' \to \gamma\eta_c(2S)$ was performed in this analysis, where $\eta_c(2S)$ was reconstructed with $K^0_S K^\pm \pi^\mp$ and $K^+K^-\pi^0$ final states. The $\eta_c(2S)$ signals are observed in the mass spectra of $K^0_S K^\pm \pi^\mp$ and $K^+K^-\pi^0$ shown in Fig. 3 with a statistical significance of greater than 10 σ under a wide range of assumptions about the signal and background properties. The data are used to obtain measurements of the $\eta_c(2S)$ mass ($M(\eta_c(2S)) = 3637.6 \pm 2.9 \pm 1.6$ MeV/c^2), width ($\Gamma(\eta_c(2S)) = 16.9 \pm 6.4 \pm 4.8$ MeV), and the product branching fraction ($\mathscr{B}(\psi' \to \gamma\eta_c(2S)) \times \mathscr{B}(\eta_c(2S) \to K\bar{K}\pi) = (1.30 \pm 0.20 \pm 0.30) \times 10^{-5}$). Combining our result with a BaBar measurement of $\mathscr{B}(\eta_c(2S) \to K\bar{K}\pi)$, we find the branching fraction of the M1 transition to be $\mathscr{B}(\psi' \to \gamma\eta_c(2S)) = (6.8 \pm 1.1 \pm 4.5) \times 10^{-4}$.

The search for $\eta_c(2S) \to \rho^0\rho^0$, $K^{*0}\bar{K}^{*0}$, and $\phi\phi$ was also performed using the same ψ' data sample [4], but no signals are observed in any of the three final states. The upper limits on the

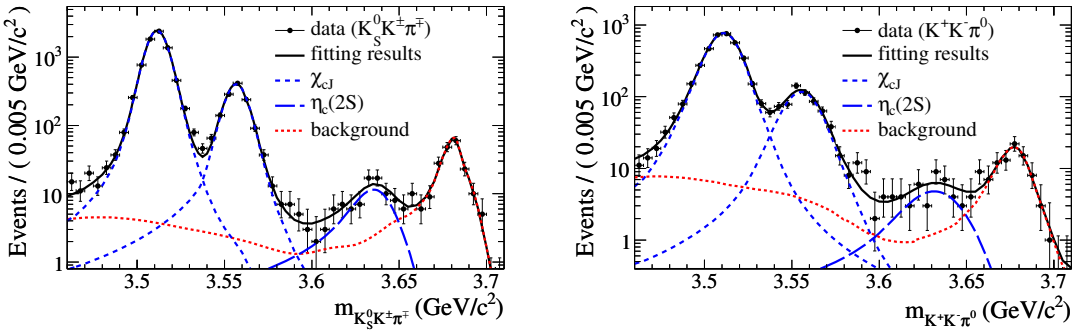

Figure 3: The invariant-mass spectrum for $K^0_S K^\pm\pi^\mp$ (left panel), $K^+K^-\pi^0$ (right panel), and the simultaneous likelihood fit to the three resonances and combined background sources as described in the text.

decay branching fractions are determined to be $\mathscr{B}(\eta_c(2S)\to\rho^0\rho^0) < 3.1\times10^{-3}$, $\mathscr{B}(\eta_c(2S)\to K^{*0}\bar{K}^{*0}) < 5.4\times10^{-3}$, and $\mathscr{B}(\eta_c(2S)\to\phi\phi) < 2.0\times10^{-3}$ at the 90% confidence level.

5. Evidence for the Direct Two-Photon Transition from ψ' to J/ψ [5]

The first measurement of the two-photon transition $\psi'\to\gamma\gamma J/\psi$ was carried out and the branching fraction is measured to be $(3.1\pm0.6(stat)^{+0.8}_{-1.0}(syst))\times10^{-4}$ using $J/\psi\to e^+e^-$ and $J/\psi\to\mu^+\mu^-$ decays. Since its statistical significance is just 3.8 σ, we also present its upper limit, 4.5×10^{-4}, at the 90% conference level. This work represents the first measurement of a two-photon transition among charmonium states. The orientation of the ψ' decay plane and the J/ψ polarization in this decay are also studied. In addition, the product branching fractions of sequential $E1$ transitions $\psi'\to\gamma\chi_{cJ}, \chi_{cJ}\to\gamma J/\psi (J=0,1,2)$ are reported.

6. Two-photon widths of the $\chi_{c0,2}$ states and helicity analysis for $\chi_{c2}\to\gamma\gamma$ [6]

The two-photon decays of $\chi_{c0,2}$ was studied via ψ' radiative decays. The clear $\chi_{c0,2}$ signals are observed in the mass spectrum of two photons shown in Fig. 4. The branching fractions are determined to be $\mathscr{B}(\chi_{c0}\to\gamma\gamma) = (2.24\pm0.19\pm0.12\pm0.08)\times10^{-4}$ and $\mathscr{B}(\chi_{c2}\to\gamma\gamma) = (3.21\pm0.18\pm0.17\pm0.13)\times10^{-4}$, which correspons the two-photon widths of $\Gamma_{\gamma\gamma}(\chi_{c0}) = (2.33\pm0.20\pm0.13\pm0.17)$ keV, $\Gamma_{\gamma\gamma}(\chi_{c2}) = (0.63\pm0.04\pm0.04\pm0.04)$ keV, and $\mathscr{R} = \Gamma_{\gamma\gamma}(\chi_{c2})/\Gamma_{\gamma\gamma}(\chi_{c0}) = 0.271\pm0.029\pm0.013\pm0.027$. The ratio of the two-photon widths for helicity $\lambda=0$ and helicity $\lambda=2$ components in the decay $\chi_{c2}\to\gamma\gamma$ is measured for the first time to be $f_{0/2} = \Gamma^{\lambda=0}_{\gamma\gamma}(\chi_{c2})/\Gamma^{\lambda=2}_{\gamma\gamma}(\chi_{c2}) = 0.00\pm0.02\pm0.02$.

7. Observation of $e^+e^-\to\eta J/\psi$ at center-of-mass energy $\sqrt{s}=4.009$ GeV

Using a 478 pb^{-1} data sample collected with the BESIII detector at a center-of-mass energy of $\sqrt{s}=4.009$ GeV, the production of $e^+e^-\to\eta J/\psi$ is observed for the first time with a statistical significance of greater than 10σ. The Born cross section is measured to be $(32.1\pm2.8\pm1.3)$ pb. Assuming the $\eta J/\psi$ signal is from a hadronic transition of the $\psi(4040)$, the fractional transition

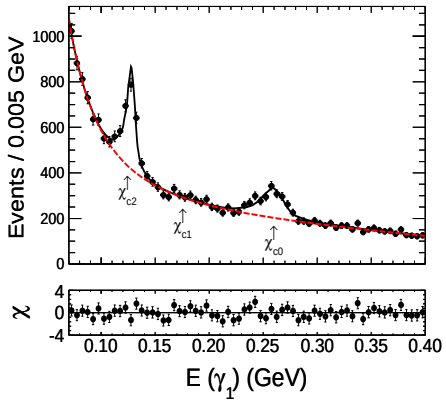

Figure 4: Upper plot: the fitted E_{γ_1} spectrum for the ψ' data sample. The expected positions of E_{γ_1} from χ_{c0}, χ_{c1}, χ_{c2} are indicated by arrows. The dashed curve shows the background line shape . Lower plot: the number of standard deviations, χ, of data points from the fitted curves.

rate is determined to be $\mathscr{B}(\psi(4040) \to \eta J/\psi) = (5.2 \pm 0.5 \pm 0.2 \pm 0.5) \times 10^{-3}$, where the first, second, and third errors are statistical, systematic, and the uncertainty from the $\psi(4040)$ resonant parameters, respectively. The production of $e^+e^- \to \pi^0 J/\psi$ is searched for, but no significant signal is observed, and $\mathscr{B}(\psi(4040) \to \pi^0 J/\psi) < 2.8 \times 10^{-4}$ is obtained at the 90% confidence level.

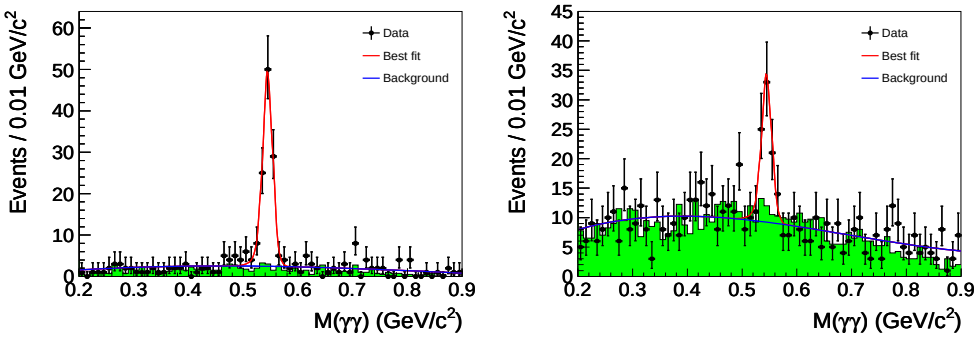

Figure 5: Distributions of $M(\gamma\gamma)$ between 0.2 GeV/c^2 and 0.9 GeV/c^2 for $J/\psi \to \mu^+\mu^-$ (left panel) and for $J/\psi \to e^+e^-$ (right panel). Dots with error bars are data in J/ψ mass signal region, and the green shaded histograms are from normalized J/ψ mass sidebands. The curves show the total fit and the background term.

8. PWA of $J/\psi \to \gamma p\bar{p}$ and $\psi' \to \gamma p\bar{p}$ [7]

Using the 225.2 million J/ψ events, we performed a full partial wave anlysis (PWA) of $J/\psi \to \gamma p\bar{p}$. The $p\bar{p}$ invariant mass distribution is shown in Fig. 6(a), where strong $p\bar{p}$ mass threshold enhancement is clearly observed. To determine its spin, parity, mass, width and production rate with high precision, the full PWA of $J/\psi \to \gamma p\bar{p}$ with $M_{p\bar{p}} < 2.2$ GeV/c^2 was performed after taking into account the final state interactions using the Julich formulation [8]. In the PWA fit the

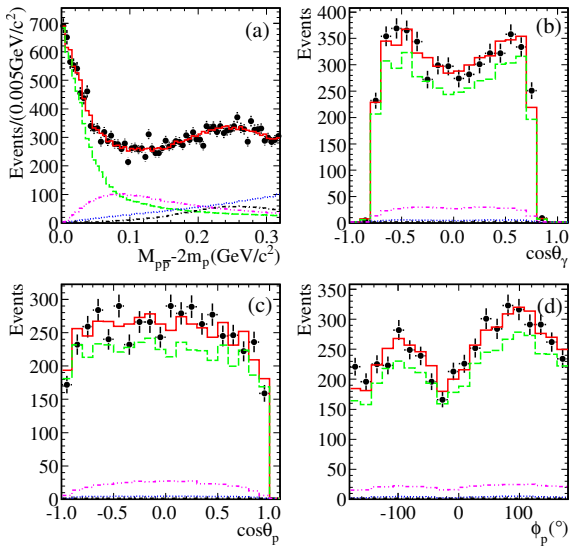

Figure 6: Comparisons between data and PWA fit projection: (a) the $p\bar{p}$ invariant mass; (b)-(d) the polar angle θ_γ of the radiative photon in the J/ψ center of mass system, the polar angle θ_p and the azimuthal angle ϕ_p of the proton in the $p\bar{p}$ center of mass system with $M_{p\bar{p}}-2m_p < 50\,\mathrm{MeV}/c^2$, respectively. Here, the black dots with error bars are data, the solid histograms show the PWA total projection, and the dashed , dotted , dash-dotted and dash-dot-dotted lines show the contributions of the $X(p\bar{p})$, 0^{++} phase space, $f_0(2100)$ and $f_2(1910)$, respectively.

$p\bar{p}$ threshold enhancement, $f_2(1910)$ and $f_0(2100)$ are described by Breit-Wigner propagators, and the parameters of the $f_2(1910)$ and $f_0(2100)$ are fixed at PDG values[9].

Figure 6 shows comparisons of the mass and angular distributions between the data and the PWA fit projections. The mass, width and product branching ratio of the $X(p\bar{p})$ are measured to be: $M = 1832^{+19}_{-5}$ (stat.)$^{+18}_{-17}$ (syst.) $\pm$ 19 (model) MeV/c^2, $\Gamma = 13 \pm 39$ (stat.)$^{+10}_{-13}$ (syst.) $\pm$ 4 (model) MeV/c^2 (a total width of $\Gamma < 76$ MeV/c^2 at the 90% C.L) and $\mathscr{B}(J/\psi \to \gamma X)B(X \to p\bar{p}) = (9.0^{+0.4}_{-1.1}$ (stat.)$^{+1.5}_{-5.0}$ (syst.) ± 2.3 (model)$) \times 10^{-5}$, respectively. For the spin-parity determination of the $X(p\bar{p})$, the 0^{-+} assignment fit is better than that for 0^{++} or other J^{PC} assignments with statistical significances that are larger than 6.8σ.

To check the contribution of $X(p\bar{p})$ in ψ' radiative decays and to measure the production ratio between J/ψ and ψ' radiative decays, A PWA on $\psi' \to \gamma p\bar{p}$ was performed and the mass and width of $X(p\bar{p})$ as well as its J^{PC} were fixed to the results obtained from J/ψ decays due to limited statistics of $\psi' \to \gamma p\bar{p}$ events. The produce branching fraction for $X(p\bar{p})$ in ψ' decay is first measured to be $\mathscr{B}(\psi' \to \gamma X) \times \mathscr{B}(X \to p\bar{p}) = (4.57 \pm 0.36$ (stat.)$^{+1.23}_{-4.07}$ (syst.) ± 1.28 (model)$) \times 10^{-6}$ and the production ratio of the $X(p\bar{p})$ between J/ψ and ψ' radiative decays is $R = (5.08^{+0.71}_{-0.45}$ (stat.)$^{+0.67}_{-3.58}$ (syst.) $\pm$ 0.12 (model)$)\%$.

9. Confirmation of X(1835) and observation of the resonances X(2120) and X(2370) [10]

In this analysis, the two decay modes of η', $\eta' \to \gamma\rho$ and $\eta' \to \pi^+\pi^-\eta$, are used to reconstruct

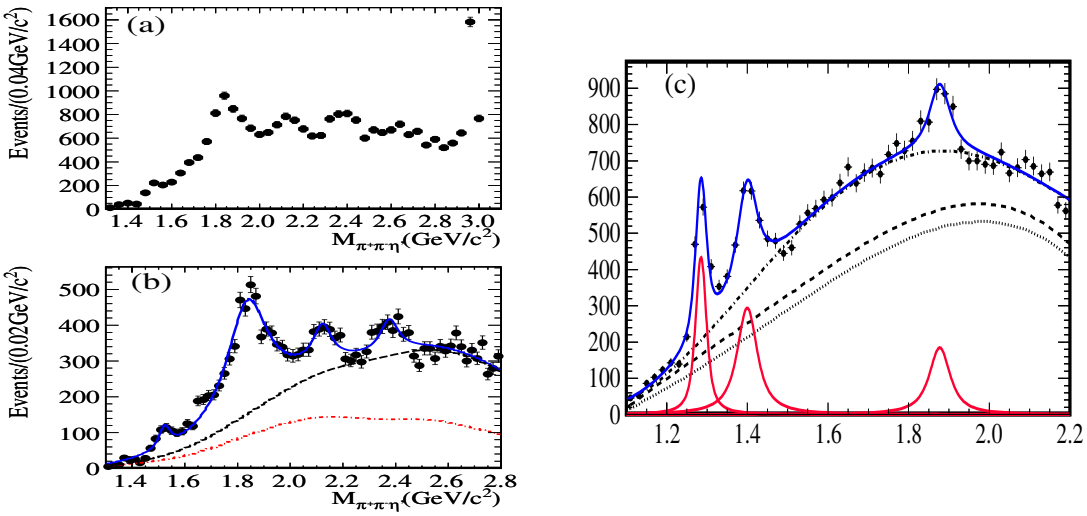

Figure 7: (a) The $\pi^+\pi^-\eta'$ invariant-mass distribution for the selected events from the two η' decay modes. (b) mass spectrum fitting with four resonances, here, the dash-dot line is contributions of non-η' events and the $\pi^0\pi^+\pi^-\eta'$ background for two η' decay modes and the dash line is contributions of the total background and non-resonant $\pi^+\pi^-\eta'$ process; (c)Results of fits to the $M(\eta\pi^+\pi^-)$ mass distribution for events with either the $\eta\pi^-$ or $\eta\pi^-$ in the $a_0(980)$ mass window. The dotted curve shows the contribution of non-ω and/or non-$a_0(980)$ background, the dashed line also includes the contribution from $J/\psi \to b_1(1235)a_0(980)$, and the dot-dashed curve indicates the total background with the non-resonant $J/\psi \to \omega a_0(980)\pi$ included. $\chi^2/d.o.f$ is 1.27 for this fit.

η', which help us cross-check our measurement, as well as obtain higher precision. Figure 7(a) and Fig. 7(b) shows the $\pi^+\pi^-\eta'$ invariant mass spectrum for the combined two η' decay modes. In addition to X(1835), a little peak corresponding to $f_1(1510)$ and two unknown structures around 2.1 GeV/c^2 and 2.4 GeV/c^2 are also observed. With the systematic uncertainties in the fit taken into account, the statistical significance of the $X(1835)$ is larger than 20σ, while those for the $f_1(1510)$, the $X(2120)$ and the $X(2370)$ are larger than 5.7σ, 7.2σ and 6.4σ, respectively. The masses and widths of X(1835), X(2120) and X(2370) are measured to be, $M_{X(1835)} = 1836.5 \pm 3.0^{+5.6}_{-2.1}$ MeV$/c^2$, $\Gamma_{X(1835)} = 190 \pm 9)^{+38}_{-36}$ MeV$/c^2$, $M_{X(2120)} = 2122.4 \pm 6.7^{+4.7}_{-2.7}$ MeV$/c^2$, $\Gamma_{X(2120)} = 83 \pm 16)^{+31}_{-11}$ MeV$/c^2$, $M_{X(2370)} = 2376.3 \pm 8.7^{+3.2}_{-4.3}$ MeV$/c^2$, $\Gamma_{X(2370)} = 83 \pm 17\ ^{+44}_{-6}$ MeV$/c^2$.

10. Observation of a resonance X(1870) in $J/\psi \to \omega\pi^+\pi^-\eta$ [11]

To look for new decay mode of X(1835), we performed the analysis of $J/\psi \to \omega\pi^+\pi^-\eta$ and observed a new structure around 1.87 GeV/c^2. The $\pi^+\pi^-\eta$ invariant mass with the requirements of either $M_{\eta\pi^+}$ or $M_{\eta\pi^-}$ in $a_0(980)$ mass region is displayed in Fig. 7(c). Three peaks corresponding to $f_1(1285)$, $\eta(1405)$ and a peak around 1.87 GeV/c^2 are clearly observed. In the fit of mass spectrum the three peaks are parametrized by efficiency-corrected Breit-Wigner functions convolved with a Gaussian resolution function. The background consists of three components, namely contributions from non-ω and/or non-$a_0(980)$ processes, $J/\psi \to b_1(1235)a_0(980)$ events, and non-resonant $\omega a_0(980)\pi$ processes. A conservative estimate of the statistical significance of X(1870) is 7.2σ, which is determined by the change of likelihood with and without the assumption

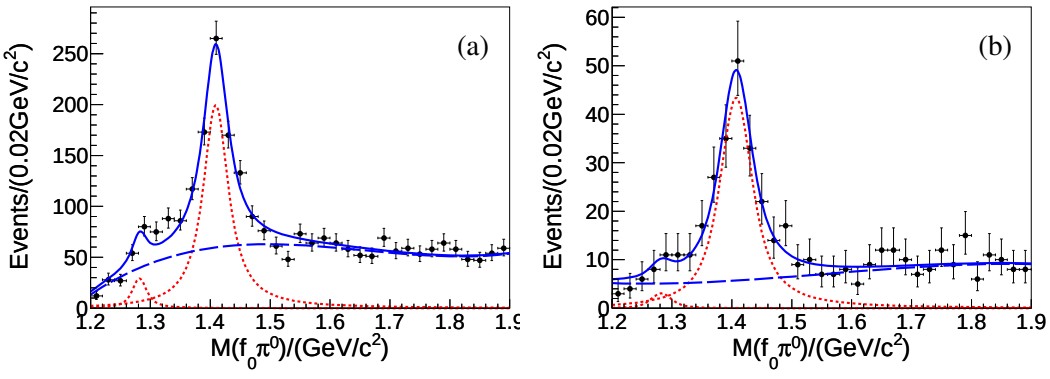

Figure 8: Results of the fit of the $f_0(980)\pi^0$ invariant mass spectrum, (a)Charged mode; (b)Neutral mode. The solid curve in the result of the fit described in the text. The dotted curve is the $f_1(1285)$ and $\eta(1405)$ signal. The dashed curves in (a) and (b) denote the background polynomial.

of X(1870). The mass, width, and the product branching ratio obtained from the fit are summarized in Table 1.

Table 1: Summary of measurements of the mass, width and the product branching ratio of $B(J/\psi \to \omega X) \times B(X \to a_0(980)\pi) \times B(a_0^{\pm}(980) \to \eta\pi^{\pm})$ where X represents $f_1(1285)$, $\eta(1405)$ and $X(1870)$.

Resonance	Mass (MeV/c^2)	Width (MeV/c^2)	$\mathscr{B}$ (10^{-4})
$f_1(1285)$	$1285.1 \pm 1.0^{+1.6}_{-0.3}$	$22.0 \pm 3.1^{+2.0}_{-1.5}$	$1.25 \pm 0.10^{+0.19}_{-0.20}$
$\eta(1405)$	$1399.8 \pm 2.2^{+2.8}_{-0.1}$	$52.8 \pm 7.6^{+0.1}_{-7.6}$	$1.89 \pm 0.21^{+0.21}_{-0.23}$
$X(1870)$	$1877.3 \pm 6.3^{+3.4}_{-7.4}$	$57 \pm 12^{+19}_{-4}$	$1.50 \pm 0.26^{+0.72}_{-0.36}$

11. First observation of $\eta(1405)$ decays into $f_0(980)\pi^0$

In this section, the results on the first observation of $\eta(1405)$ decays into $f_0(980)\pi^0$ in $J/\psi \to \gamma\pi^+\pi^-\pi^0$ and $J/\psi \to \gamma\pi^0\pi^0\pi^0$ is presented. The mass spectra of $\pi^+\pi^-\pi^0$ and $\pi^0\pi^0\pi^0$ are shown in Fig. 8, where a prominent $\eta(1405)$ peak and an evident bump around 1.3 GeV/c^2 regarded as $f_1(1285)$ are observed. In the fit the two peaks are parameterized by efficiency-corrected Breit-Wigner functions convolved with a Gaussian resolution function in which the mass and width of $f_1(1285)$ is fixed at PDG values. A third order Chebychev polynomial is described for the background events, of which the shape parameters are determined from a simultaneous fit to the $\pi^+\pi^-\pi^0$ mass spectrum where $\pi^+\pi^-$ is in the $f_0(980)$ sidebands. The mass, width, and the product branching ratios of $\eta(1405)$ and $f_1(1285)$ obtained from the fit are listed in Table 2. Since the statistical significance of $f_1(1285) \to \pi^0\pi^0\pi^0$ is only 1.2σ. Therefore an upper limit of the branching fraction at 90% confidence level is given.

12. PWA of $J/\psi \to \gamma\eta\eta$ [13]

A full partial wave analysis on $J/\psi \to \gamma\eta\eta$ was performed using the relativistic covariant

Table 2: Summary of measurements of the mass, width and the product branching ratio of $Br(J/\psi \to \gamma X \to \gamma\pi^0 f_0(980) \to \gamma 3\pi)$.

Resonance	M(MeV/c^2)	Γ(MeV/c^2)	$\mathscr{B}(10^{-6})$
$\eta(1405)(\pi^+\pi^-\pi^0)$	1409.0 ± 1.7	48.3 ± 5.2	$15.0 \pm 1.1 \pm 1.1$
$f_1(1285)(\pi^+\pi^-\pi^0)$	fixed	fixed	$1.0 \pm 0.3 \pm 0.1$
$\eta(1405)(\pi^0\pi^0\pi^0)$	1407.0 ± 3.5	55.0 ± 11.0	$7.1 \pm 0.8 \pm 0.8$
$f_1(1285)(\pi^0\pi^0\pi^0)$	fixed	fixed	< 0.7

tensor amplitude method and the results are summarized in Table 3. The scalar contributions are mainly from $f_0(1500)$, $f_0(1710)$ and $f_0(2100)$, while no evident contributions from $f_0(1370)$ and $f_0(1790)$ are seen. Recently, the production rate of the pure gauge scalar glueball in J/ψ radiative decays predicted by the lattice QCD [14] was found to be compatible with the production rate of J/ψ radiative decays to $f_0(1710)$; this suggests that $f_0(1710)$ has a larger overlap with the glueball compared to other glueball candidates (eg. $f_0(1500)$). In this analysis, the production rate of $f_0(1710)$ and $f_0(2100)$ are both about one order of magnitude larger than that of the $f_0(1500)$ and no clear evidence is found for $f_0(1370)$, which are both consistent with, at least not contrary to, lattice QCD predictions.

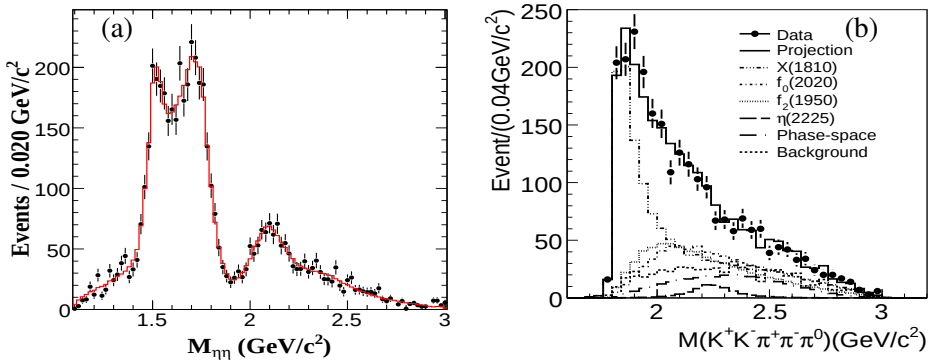

Figure 9: Comparisons between data and PWA fit projections: (a) the mass spectrum of $\eta\eta$; (b) the mass spectrum of $\omega\phi$.

The tensor components, which are dominantly from $f_2'(1525)$, $f_2(1810)$ and $f_2(2340)$, also have a large contribution in $J/\psi \to \gamma\eta\eta$ decays. The significant contribution from $f_2'(1525)$ is shown as a clear peak in the $\eta\eta$ mass spectrum; a tensor component exists in the mass region from 1.8 GeV/c^2 to 2 GeV/c^2, although we cannot distinguish $f_2(1810)$ from $f_2(1910)$ or $f_2(1950)$; and the PWA requires a strong contribution from $f_2(2340)$, although the possibility of $f_2(2300)$ cannot be ruled out.

13. PWA of $J/\psi \to \gamma\omega\phi$ [15]

A study of the doubly OZI suppressed decays of $J/\psi \to \gamma\omega\phi$ is performed and a strong deviation ($> 30\sigma$) from three-body $J/\psi \to \gamma\omega\phi$ phase space is observed near the $\omega\phi$ mass threshold shown in Fig. 9 that is consistent with a previous observation reported by the BESII experiment. A partial wave analysis with a tensor covariant amplitude that assumes that the enhancement is

Table 3: Summary of the PWA results for $J/\psi \to \gamma\eta\eta$.

Resonance	Mass(MeV/c^2)	Width(MeV/c^2)	$\mathscr{B}(J/\psi \to \gamma X \to \gamma\eta\eta)$	Significance
$f_0(1500)$	1468^{+14+23}_{-15-74}	$136^{+41+28}_{-26-100}$	$(1.65^{+0.26+0.51}_{-0.31-1.40}) \times 10^{-5}$	8.2 σ
$f_0(1710)$	$1759\pm6^{+14}_{-25}$	$172\pm10^{+32}_{-16}$	$(2.35^{+0.13+1.24}_{-0.11-0.74}) \times 10^{-4}$	25.0 σ
$f_0(2100)$	$2081\pm13^{+24}_{-36}$	273^{+27+70}_{-24-23}	$(1.13^{+0.09+0.64}_{-0.10-0.28}) \times 10^{-4}$	13.9 σ
$f_2'(1525)$	$1513\pm5^{+4}_{-10}$	75^{+12+16}_{-10-8}	$(3.42^{+0.43+1.37}_{-0.51-1.30}) \times 10^{-5}$	11.0 σ
$f_2(1810)$	1822^{+29+66}_{-24-57}	$229^{+52+88}_{-42-155}$	$(5.40^{+0.60+3.42}_{-0.67-2.35}) \times 10^{-5}$	6.4 σ
$f_2(2340)$	$2362^{+31+140}_{-30-63}$	$334^{+62+165}_{-54-100}$	$(5.60^{+0.62+2.37}_{-0.65-2.07}) \times 10^{-5}$	7.6 σ

due to the presence of a resonance, the $X(1810)$, is performed, and confirms that the spin-parity of the $X(1810)$ is 0^{++}. The mass and width of the $X(1810)$ are determined to be $M = 1795 \pm 7(\text{stat})^{+13}_{-5}(\text{syst})\pm19(\text{mod})$ MeV/c^2 and $\Gamma = 95 \pm 10(\text{stat})^{+21}_{-34}(\text{syst})\pm75(\text{mod})$ MeV/c^2, respectively, and the product branching fraction is measured to be $\mathscr{B}(J/\psi \to \gamma X(1810)) \times \mathscr{B}(X(1810) \to \omega\phi) = (2.00 \pm 0.08(\text{stat})^{+0.45}_{-1.00}(\text{syst})\pm1.30(\text{mod}))\times10^{-4}$. These results are consistent within errors with those of the BESII experiment.

14. PWA of $\psi' \to p\bar{p}\pi^0$ [16]

Based on $106\times10^6\,\psi'$ events collected with the BESIII detector at the BEPCII facility, a partial wave analysis of $\psi' \to p\bar{p}\pi^0$ is performed. The branching fraction of this channel has been determined to be $B(\psi(3686) \to p\bar{p}\pi^0) = (1.65 \pm 0.03 \pm 0.15) \times 10^{-4}$. In this decay, 7 N^* intermediate resonances are observed. Among these N^* resonances, two new resonances are significant, one $1/2^+$ resonance with a mass of $2300^{+40+109}_{-30-0}$ MeV/c^2 and width of $340 \pm 30^{+110}_{-58}$ MeV/c^2, and one $5/2^-$ resonance with a mass of 2570^{+19+34}_{-10-10} MeV/c^2 and width of 250^{+14+69}_{-24-21} MeV/c^2. For the remaining 5 N^* intermediate resonances, the analysis yields mass and width values which are consistent with those from established resonances.

Table 4: Summary of the PWA results for $\psi' \to p\bar{p}\pi^0$.

Resonance	M(MeV/c^2)	Γ(MeV/c^2)	ΔS	ΔN_{dof}	Sig.
$N(1440)$	1390^{+11+21}_{-21-30}	$340^{+46+70}_{-40-156}$	72.5	4	11.5σ
$N(1520)$	1510^{+3+11}_{-7-9}	115^{+20+0}_{-15-40}	19.8	6	5.0σ
$N(1535)$	1535^{+9+15}_{-8-22}	120^{+20+0}_{-20-42}	49.4	4	9.3σ
$N(1650)$	1650^{+5+11}_{-5-30}	150^{+21+14}_{-22-50}	82.1	4	12.2σ
$N(1720)$	1700^{+30+32}_{-28-35}	$450^{+109+149}_{-94\ -44}$	55.6	6	9.6σ
$N(2300)$	$2300^{+40+109}_{-30-0}$	$340^{+30+110}_{-30-58}$	120.7	4	15.0σ
$N(2570)$	2570^{+19+34}_{-10-10}	250^{+14+69}_{-24-21}	78.9	6	11.7σ

15. Semileptonic D decays: $D^0 \to K^-e^+\nu$ and $\pi^-e^+\nu$

The semileptonic D decay measurements are a good laboratory for testing theories of QCD.

The BESIII experiment has taken about 2.9 fb^{-1} data at open-charm threshold during the 2010 and 2011 data runs. Using one-third of the data, a partially-blind analysis has been done with the $D^0 \to Ke\nu$ and $D^0 \to \pi e\nu$ decays. The signal events with a missing ν are inferred using the variable $U = E_{miss} - |P_{miss}|$, similar to missing mass square, where "miss" here refers to the missing energy or momentum. Figure 10 shows the U distributions and fit projections for the decays of $\bar{D}^0 \to K^+e^-\nu$ and $\bar{D}^0 \to \pi^+e^-\nu$.

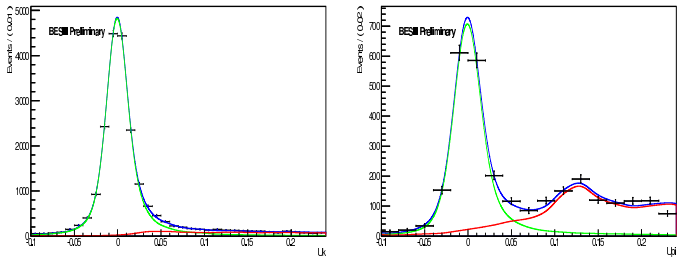

Figure 10: U distributions of $\bar{D}^0 \to K^+e^-\nu$(left) and $\bar{D}^0 \to \pi^+e^-\nu$(right). Blue, green, and red curves are the total fit, signal fit, and background fit, respectively.

Given the signal yields obtained from fitting U distributions and signal efficiencies obtained from signal Monte Carlo, the absolute branching fractions are measured to be $\mathscr{B}(\bar{D}^0 \to K^+e^-\nu) = (3.542 \pm 0.030 \pm 0.067)\%$ and $\mathscr{B}(\bar{D}^0 \to \pi^+e^-\nu) = (0.288 \pm 0.008 \pm 0.005)\%$, which are consistent with the previous measurements from CLEO-c [17].

16. Rare charm decays at BESIII: preliminary results on $D^0 \to \gamma\gamma$

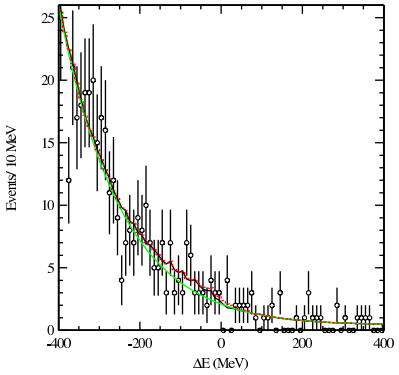

Figure 11: A fit to the $D^0 \to \gamma\gamma$ candidate ΔE distribution based on the $\psi(3770)$ data sample. Black points are data, solid black curve is the overall fitted curve (signal plus backgrounds), the red-dashed curve is the fitted total background, and the green curve is the exponential and linear polynomials.

With 2.9 fb^{-1} data at $\psi(3770)$ peak, we analyze $D^0 \to \gamma\gamma$, and Fig. 11 shows ΔE distribution, where ΔE is the energy difference between reconstructed energy of D meson and beam energy. The signal candidates should be peak near zero, therefore, no significant signal events are observed. We

perform a maximum-likelihood fit to the ΔE distribution. In the fit, the signal shape is fixed by the corresponding MC shape. The background shape consists of three parts; MC-based shape to represent the contamination from $D^0 \to \pi^0\pi^0$ whose size is also fixed based on our own observation; a 1st order polynominal that covers the contamination from Bhabha events which appear smoothly over the entire ΔE spectrum; a 1st order exponential polynominal, corresponding to the rest of the backgrounds. The fit yields -2.9 ± 7.1 signal events. This translates into an upper limit of 11 events at 90% C.L. based on the Bayesian method. Including the estimated total systematic uncertainty, we arrive at $\mathscr{B}(D^0 \to \gamma\gamma)/\mathscr{B}(D^0 \to \pi^0\pi^0) < 5.8 \times 10^{-3}$ at 90% C.L.. With the known value of $\mathscr{B}(D^0 \to \pi^0\pi^0)$ [9], this corresponds to $\mathscr{B}(D^0 \to \gamma\gamma) < 4.7 \times 10^{-6}$.

17. Summary

Based on the samples of 106 million ψ', 225 million J/ψ events and $2.9 fb^{-1}$ data taken 3.773 GeV, the recent results on charmonium decays, light hadron spectroscopy and charm decays are presented, which illustrate the rich physics in the τ-charm region. More promising results, in particular the charm physics, are expected to be coming soon.

References

[1] M. Ablikim *et al.* (BESIII Collaboration), Phys. Rev. Lett **108**, 222002 (2012).

[2] M. Ablikim *et al.* (BESIII Collaboration), Phys. Rev. Lett. **104**, 132002 (2010).

[3] M. Ablikim *et al.* (BESIII Collaboration), Phys. Rev. Lett. **109**, 042003 (2012).

[4] M. Ablikim *et al.* (BESIII Collaboration), Phys. Rev. **D 84**, 091102 (2011).

[5] M. Ablikim *et al.* (BESIII Collaboration), Phys. Rev. Lett. **109**, 172002 (2012).

[6] M. Ablikim *et al.* (BESIII Collaboration), Phys. Rev. **D 85**, 112008 (2012).

[7] M. Ablikim *et al.* (BESIII Collaboration), Phys. Rev. Lett. **108**, 112003 (2012).

[8] A. Sirbirtsen *et al.*, Phys. Rev. **D 71**,054010 (2005).

[9] J. Beringer *et al.* (Particle Data Group), Phys. Rev. D **86**, 010001 (2012).

[10] M. Ablikim *et al.* (BESIII Collaboration), Phys. Rev. Lett. **106**, 072002 (2011).

[11] M. Ablikim *et al.* (BESIII Collaboration), Phys. Rev. Lett. **107**, 182001 (2011).

[12] K. Nakamura *et al.* (Particle Data Group), J. Phys. G **37**, 075021 (2010).

[13] M. Ablikim *et al.* (BESIII Collaboration), arXiv:1301.0051.

[14] L. C. Gui *et al.*, Phys.Rev.Lett. **110**, 021601 (2013).

[15] M. Ablikim *et al.* (BESIII Collaboration), arXiv:1211.5668.

[16] M. Ablikim *et al.* (BESIII Collaboration), arXiv:1207.0223.

[17] D. Besson *et al.* (CLEO Collaboration), Phys. Rev. **D 80**, 032005 (2009).